Chem

CellPress
OPEN ACCESS

Article

Stereodynamics of *E*/*Z* isomerization in rotaxanes through mechanical shuttling and covalent bond rotation

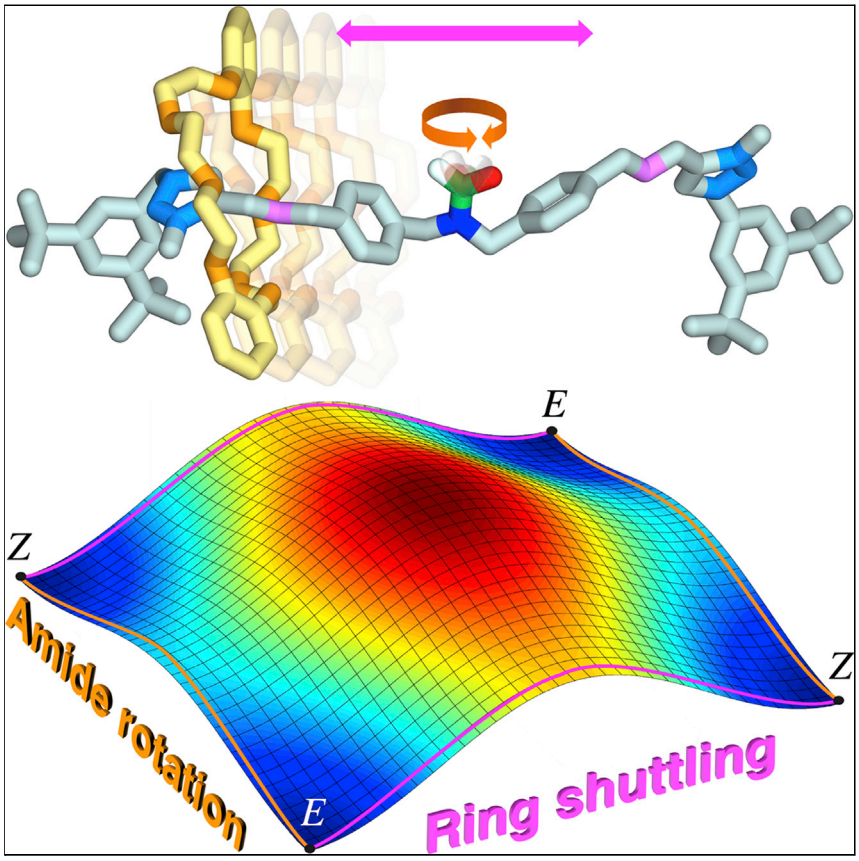

We report on a set of rotaxanes with symmetrical axles equipped with a central amide group that installs *E*/*Z* stereoisomerism owing to the ring position along the axle. Isomerization by concomitant rotation about the amide bond and ring shuttling along the axle was thoroughly characterized in different solvents. The results trigger a discussion on core concepts, such as microscopic reversibility and transition state theory, and provide insights for designing molecules capable to transform and transmit motion between subcomponents.

Stefano Corra, Christiaan de Vet, Massimo Baroncini, Alberto Credi, Serena Silvi

massimo.baroncini@unibo.it (M.B.)
alberto.credi@unibo.it (A.C.)

Highlights

Rotaxanes that display *E*/*Z* stereoisomerism depending on the ring position

Co-existence of two different stereomutations that yield the same product

Mutual influence and opposite solvent dependence of the two dynamic processes

Fundamental implications for microscopic reversibility and chemical equilibrium

Corra et al., Chem 7, 2137–2150
August 12, 2021
https://doi.org/10.1016/j.chempr.2021.04.010

Chem

CellPress
OPEN ACCESS

Article

Stereodynamics of *E/Z* isomerization in rotaxanes through mechanical shuttling and covalent bond rotation

Stefano Corra,[1,2] Christiaan de Vet,[1,3] Massimo Baroncini,[1,3,*] Alberto Credi,[1,2,5,*] and Serena Silvi[1,4]

SUMMARY

The mechanical bond has opened a new world for structural and dynamic stereochemistry, which is still largely underexplored and whose significance for various applications is becoming increasingly evident. We demonstrate that designed rearrangements involving both covalent and mechanical bonds can be integrated in [2]rotaxanes, leading to interesting consequences in terms of *E/Z* isomerization mechanisms. Two entirely distinct and concomitant stereomutations, pertaining to the same stereogenic element but involving different kinds of linkages within the molecule, are observed and are thoroughly characterized. The rate of the two processes is affected in opposite ways upon changing solvent polarity; such a phenomenon can be used to selectively modify the rate of each motion and adjust the relative contribution of the two mechanisms to the isomerization. Although the movements are not synchronized, an analysis of the intriguing fundamental implications for transition state theory, reaction pathway bifurcation, and microscopic reversibility was triggered by our experimental observations.

INTRODUCTION

The introduction of the mechanical bond as a new form of molecular linkage has noticeably contributed to enliven contemporary stereochemistry,[1] an old science whose first practitioner was Louis Pasteur.[2,3] Indeed, the practical and theoretical investigation of mechanically interlocked molecules (MIMs) has unveiled a stereochemical Pandora's box, leading to the discovery of unprecedented forms of "static"—orientational,[4] translational,[5] and sequence[6] isomerism, and mechanical and topological chirality[7]—and "dynamic" stereoisomerism—translation and circumrotation,[8] pirouetting,[9] and rocking.[10] At present, the study of the stereochemistry of MIMs, i.e., mechano-stereochemistry, represents one of the most intellectually challenging lines of research in fundamental chemistry. This area is teeming with opportunities, not only as a consequence of the vastness of its scope but also for the growing role of MIMs in the development of new catalysts,[11–14] advanced materials,[15–18] and molecular machines.[1,19–23]

In recent years, the investigation of enantiomerism in MIMs, owing to the central role of chirality in chemistry, has been the main focus of investigations in mechano-stereochemistry,[11–14,24–26] while other forms of stereoisomerism have attracted relatively less attention.[27] In particular, the static and dynamic aspects of *cis-trans* isomerism in rotaxanes—MIMs minimally composed of a macrocyclic ring encircling an axle-like molecule endowed with bulky end groups too large to pass through the ring opening—are largely unexplored.

The bigger picture

The concurrence and interplay of different movements of molecular components within the same structure play a key role in providing function to naturally occurring molecular machines. Despite the progress made on artificial counterparts, the construction of molecular systems, where two (or more) motions are integrated together to produce an outcome, is still in its infancy. Molecules called rotaxanes, obtained by interlocking a ring with a dumbbell-shaped axle, are an appealing yet underexplored platform for this purpose. Here, we describe rotaxanes where two coexisting and radically different processes—rotation about a covalent bond and translation of the ring along the axle—lead to the same change in the overall molecular shape. These results are significant not only to improve our fundamental understanding of the way molecular components move but also to develop sophisticated artificial nanomachines capable of transforming or transmitting motion.

In this context, let us consider a molecular axle divided into two identical halves by a covalent bond linking the axle to two different substituents, A and B, such that all the substituents attached to the bond lie on the same plane (Figure 1A). Even if the rotation about this covalent bond is hindered, such a molecule cannot exhibit geometrical isomerism, as it does not satisfy the necessary and sufficient condition of having one substituent different from the other at each end of the bond. On the other hand, in a [2]rotaxane obtained by interlocking such as an axle with a macrocycle[28] (Figure 1B), the two halves of the axle component become different, as long as the ring is stationing on either side of the axle with respect to the midpoint, thus introducing *cis-trans* isomerism.[29] Therefore, geometrical isomerism emerges as a consequence of the mechanical linkage between the ring and the axle components in the assembled rotaxane.

Rotaxanes of this kind were first reported by Vögtle in the 90s[30] but received only incidental attention afterwards,[31,32] and their stereodynamic behavior has never been analyzed in detail. In particular, it has apparently been overlooked[33] that, in principle, these architectures can undergo *E*/*Z* isomerization through three distinct paths: (1) conformational isomerization via rotation about the covalent bond at the center of the axle, (2) co-conformational "mechanical" isomerization via ring shuttling, and (3) degenerate isomerization (i.e., an automerization reaction)[34] via concerted bond rotation and ring shuttling movements (Figure 1C). The presence of mechanistically distinct and entirely different isomerization paths that, in principle, could take place simultaneously represents an extremely rare occurrence in chemistry, seldom experimentally verified in small molecules[35] and metal complexes,[36,37] and never described in MIMs. Furthermore, the possibility of a concerted automerization path, which would entail an interplay between the rotational and mechanical shuttling motion, is interesting because geared molecular movements not only represent a fundamental consequence of stereoisomeric transformations[38] but also play a key role in the development of advanced molecular devices and machines.[1,19,39–42]

RESULTS AND DISCUSSION

The opportunity to investigate unexplored aspects of MIMs stereodynamics prompted us to synthesize and study a family of [2]rotaxanes that exhibit *cis-trans* isomerism due to the presence of a bond with restricted rotation on their axle component (Figure 1). Such species need to be designed considering that the two distinct isomerization processes should be monitored independently and occur on experimentally accessible timescales in the temperature range allowed by solution measurements. These considerations led us to make rotaxanes $\mathbf{1}^{2+}$ and $\mathbf{2}^{2+}$ (Scheme 1), whose axle component is constituted by two symmetrically positioned triazolium units bridged either by a formyl (in $\mathbf{1}^{2+}$) or an acetyl (in $\mathbf{2}^{2+}$) dibenzylamide moiety, and is terminated at both extremities by bulky di-*tert*-butylbenzyl stopper groups. Dibenzo[24]crown8 (DB24C8) was selected as the ring component. The triazolium units are recognition sites for DB24C8[43] and offer two equivalent low energy "parking" positions for the ring situated on opposite sides of the central dibenzylamide unit.[24] Thus, in order to shuttle between the triazolium stations, the macrocycle has to pass over the formyl ($\mathbf{1}^{2+}$) or acetyl ($\mathbf{2}^{2+}$) group.

Because of the restricted rotation about the amide CN–CO bond,[44–46] rotaxanes $\mathbf{1}^{2+}$ and $\mathbf{2}^{2+}$ are expected to occur as a pair of diastereoisomers, namely, *E*-$\mathbf{1}^{2+}$/*Z*-$\mathbf{1}^{2+}$ and *E*-$\mathbf{2}^{2+}$/*Z*-$\mathbf{2}^{2+}$, distinguished by the relative position of the macrocycle and the carbonyl group of the amide unit. Scheme 1 illustrates the structures and the

[1]CLAN-Center for Light Activated Nanostructures, Istituto ISOF-CNR, via Gobetti 101, 40129 Bologna, Italy

[2]Dipartimento di Chimica Industriale "Toso Montanari," Università di Bologna, viale del Risorgimento 4, 40136 Bologna, Italy

[3]Dipartimento di Scienze e Tecnologie Agro-Alimentari, Università di Bologna, viale Fanin 44, 40127 Bologna, Italy

[4]Dipartimento di Chimica "G. Ciamician," Università di Bologna, via Selmi 2, 40126 Bologna, Italy

[5]Lead contact

*Correspondence: massimo.baroncini@unibo.it (M.B.), alberto.credi@unibo.it (A.C.)

https://doi.org/10.1016/j.chempr.2021.04.010

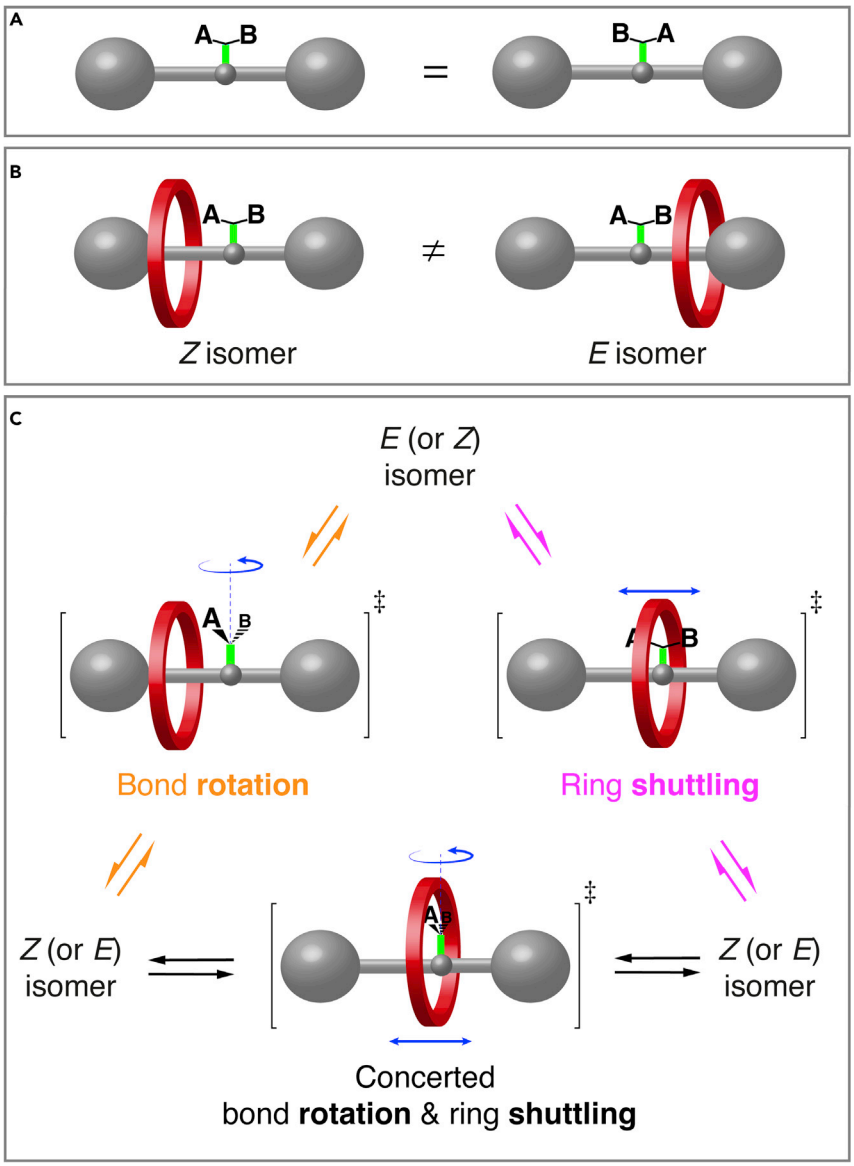

Figure 1. Combination of covalent and mechanical movements in a [2]rotaxane

(A) Schematic representation of a molecular axle divided into two identical halves by a covalent bond (in green) linking two different substituents, A and B, and exhibiting restricted rotation. Rotation about the green bond yields the same molecule.

(B) The pair of *E*/*Z* stereoisomers that results from the interlocking of the axle shown in (A) with a macrocyclic ring to afford a [2]rotaxane.

(C) Schematics of the isomerization mechanisms that can happen in the [2]rotaxane, and simplified representation of the traversed transition states: bond rotation (orange), ring shuttling (magenta), and concerted bond rotation/ring shuttling (black). The corresponding molecular movements are highlighted by the blue arrows. While either bond rotation or ring shuttling leads to a different stereoisomer, the isomer obtained upon concerted rotation/shuttling is the same as the starting one.

possible interconversion processes of the *E*/*Z* stereoisomers of $\mathbf{1}^{2+}$ and $\mathbf{2}^{2+}$, namely, (1) rotation of the carbonyl residue about the CN–CO bond, (2) shuttling of the crown ether between the triazolium stations, and (3) concerted amide bond rotation and shuttling.

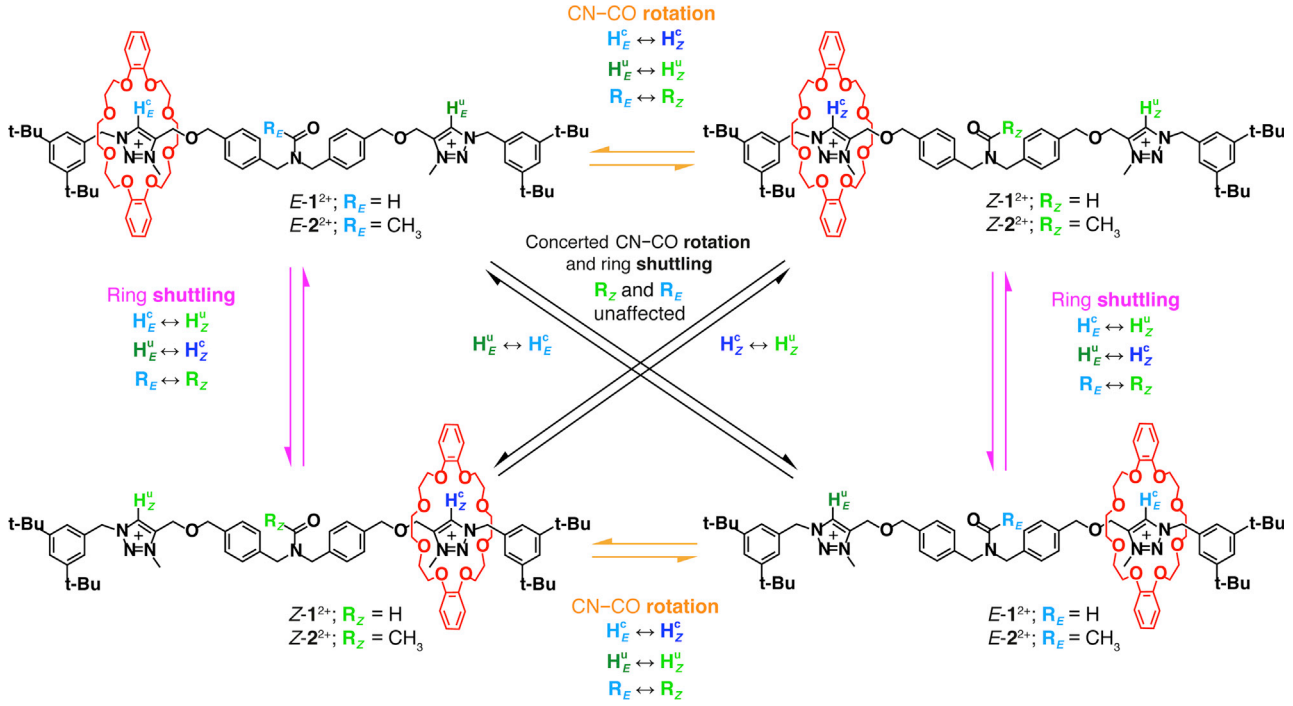

Scheme 1. Molecular structure and isomerization processes of rotaxanes 1^{2+} and 2^{2+}

Both species exist as two geometrical stereoisomers. The isomerization reactions via CN–CO bond rotation or ring shuttling and the degenerate isomerization reaction via concerted CN–CO bond rotation and ring shuttling are represented. Diagnostic protons are color coded, and their intersite exchange pattern, as a result of the different isomerization processes, is indicated.

1^{2+} and 2^{2+} were synthesized in excellent yields as PF_6^- salts upon formylation or acetylation of the dibenzylamine moiety of a common [2]rotaxane precursor (Schemes S1 and S2). The dibenzylamine moiety is the remnant of a secondary ammonium center employed to thread the ring prior to the stoppering, as the triazolium unit is a too weak recognition site to template rotaxane formation.[47] On the other hand, the low affinity of DB24C8 for the triazolium stations prevents a tight trapping of the ring on either station, which is a key requirement to enable shuttling at relatively low temperatures.[24,48] The ^{1}H NMR spectra of both 1^{2+} and 2^{2+} in DMSO-d_6 at 298 K (Figure 2) present four distinguishable singlets in the region between 8.5 and 9.5 ppm. These were assigned, through careful 2D NMR experiments (Figures S1, S20, and S21), to the triazolium protons of the *E* and *Z* stereoisomer, which are encircled (H^c_E and H^c_Z) or not encircled (H^u_E and H^u_Z) by the ring. The formyl proton in 1^{2+} and the acetyl protons in 2^{2+} are also present as a couple of singlets at about 8.4 ppm and 2.1 ppm, respectively. Their occurrence as two sets of resonances is the result of the two possible orientations, toward (R_E) or away from (R_Z) the macrocycle, associated with the *E*- and *Z*-isomers, respectively (Figure 2). A comparison between the integral ratio of the proton resonances of the *E*- and *Z*-amide stereoisomers revealed that in 1^{2+} and 2^{2+} the two isomeric forms are equally populated within errors in both polar and apolar media.

These observations prove that, as entailed by their design, in both rotaxanes the macrocycle resides on one of the two triazolium stations, thus differentiating the two sides of the axle and giving rise to a pair of distinct *E* and *Z* stereoisomers. Moreover, the fact that they are present in the same amount indicates that the orientation of the acyl substituent does not significantly affect the affinity between the ring and

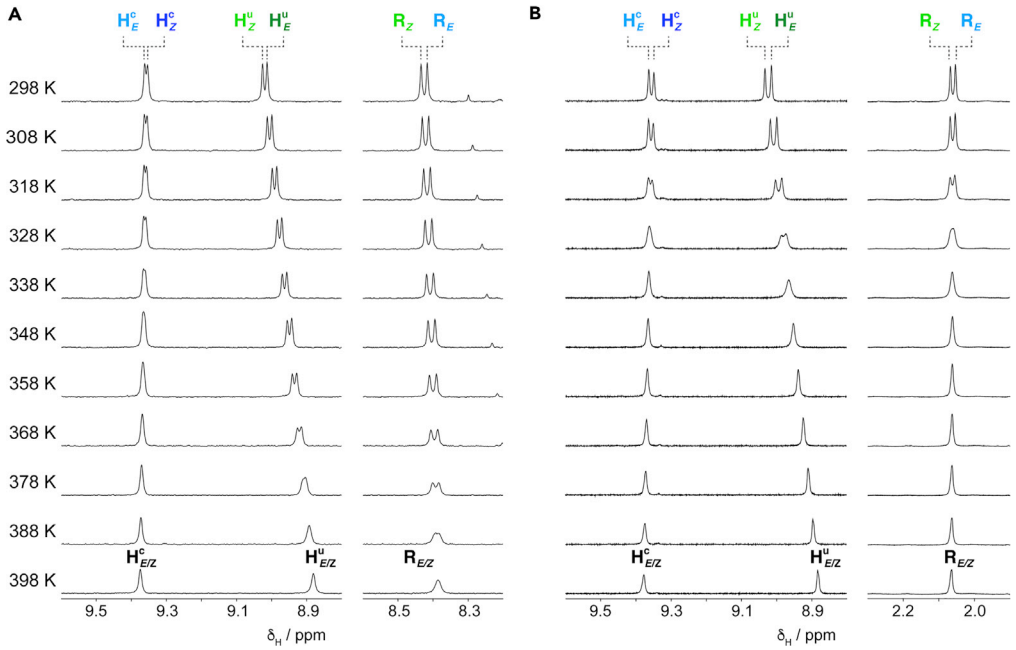

Figure 2. Rotaxane dynamics probed by NMR spectroscopy

Partial variable temperature (VT) ^{1}H NMR spectra (500 MHz, DMSO-d_6) of $\mathbf{1}^{2+}$ (A) and $\mathbf{2}^{2+}$ (B) in the regions of the triazolium protons (H^c_E, H^c_Z, H^u_E, H^u_Z; left) and of the amide protons (R_E, R_Z; right, R = H for $\mathbf{1}^{2+}$ and CH_3 for $\mathbf{2}^{2+}$). For protons labeling refer to Scheme 1.

the triazolium stations. Finally, the presence of a distinct set of well-resolved proton signals for each stereoisomer is a clear evidence that all possible exchange paths are either inactive or slow in the ^{1}H NMR timescale at room temperature (see Scheme 1). A slow exchange regime for the rotation about the CN–CO bond of the formyl and acetyl residues is not unexpected, since it is commonly observed in analogous amides in similar conditions.[44–46] Likewise, a slow shuttling motion of the ring between the triazolium stations is consistent with the observation that even the small formyl group greatly increases the shuttling energy barrier in analogous rotaxanes.[33] Nonetheless, the progressive broadening and coalescence of the signals in the ^{1}H NMR spectra of both $\mathbf{1}^{2+}$ and $\mathbf{2}^{2+}$ with increasing temperature (Figures 2 and S2–S9; Table S1) clearly reveals the presence of an exchange dynamic involving the different isomeric forms.

To comprehend which one(s) of the different possible isomerization mechanisms is(are) active, it is important to consider that, taken individually, both rotation about the CN–CO bond and shuttling of the ring between the triazolium stations directly interconvert the *E*- and *Z*-isomers of $\mathbf{1}^{2+}$ and $\mathbf{2}^{2+}$. Thus, these two processes must lead to an exchange of *every* peak in the NMR spectrum of one stereoisomer with its counterpart in the other (Scheme 1). On the contrary, the synchronous rotation-shuttling path represents an automerization reaction, which transforms the *E*- or *Z*-isomer of either rotaxanes in the same isomer. A geared shuttling-rotation mechanism will, therefore, exchange only some of the signals of either stereoisomer and should have no effect on the signals of protons whose environment is unchanged, i.e., those of the formyl and acetyl protons (R_E and R_Z), respectively, in $\mathbf{1}^{2+}$ and $\mathbf{2}^{2+}$ (Scheme 1).[49] Although these differences should, in principle, allow to identify the active path(s) using the total line shape analysis of variable temperature ^{1}H NMR experiments,[50] the relatively high symmetry of $\mathbf{1}^{2+}$ and $\mathbf{2}^{2+}$ leads to spectral signals, which consent to formulate only generic hypotheses on the underlying exchange

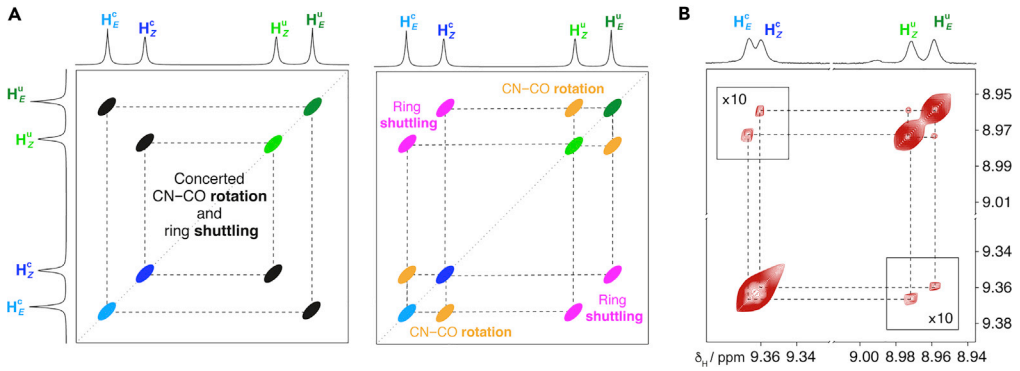

Figure 3. Identification of the isomerization mechanisms

(A) Predicted ^{1}H NMR EXSY cross-peaks of the triazolium protons for the concerted CN–CO rotation/ring shuttling (left), and for pure CN–CO bond rotation or ring shuttling isomerization reactions (right) of $\mathbf{1}^{2+}$ and $\mathbf{2}^{2+}$.

(B) Partial EXSY ^{1}H NMR spectrum of $\mathbf{1}^{2+}$ (500 MHz, DMSO-d_6, 333 K, t_{mix} = 200 ms).

process(es). In particular, while the common coalescence temperature of proton resonances with a similar frequency difference in $\mathbf{2}^{2+}$ suggests that only one path is active, the slightly different coalescence temperature of $H^{u}_{E/Z}$ and $R_{E/Z}$ in $\mathbf{1}^{2+}$ is consistent with different exchange processes occurring at similar rates.

To get a better insight into the active isomerization processes in the explored temperature range, we performed two-dimensional NMR exchange spectroscopy (EXSY) experiments (Figure S11).[51] In EXSY spectra, the in-phase cross-peaks contain information about intersite chemical exchange and enable to unambiguously identify which one(s) of the different processes is(are) occurring. In particular, cross-peaks between the signals of H^{u}_{E}, H^{c}_{E} and H^{u}_{Z}, H^{c}_{Z} are expected for a concerted mechanism, with no cross-peaks between the proton resonances of the *E*- and *Z*-isomers as required by an automerization path (Figure 3A, left). Conversely, a rotation mechanism would exchange H^{u}_{E} with H^{u}_{Z} and H^{c}_{E} with H^{c}_{Z}, whereas a shuttling motion of the ring would put in correlation H^{u}_{E} with H^{c}_{Z} and H^{u}_{Z} with H^{c}_{E}, as expected for reaction paths that directly interconvert *E*- and *Z*-isomers (Figure 3A, right). The EXSY spectrum of $\mathbf{1}^{2+}$ recorded at 333 K with a mixing time of 200 ms (Figure 3B) clearly reveals a pattern of cross-peaks consistent with both CN–CO bond rotation and ring shuttling occurring as separate but concomitant events, thus ruling out a concerted mechanism. Conversely, the EXSY spectra of $\mathbf{2}^{2+}$ present only the cross-peaks associated with CN–CO bond rotation; ring shuttling is not observed even at the highest temperature (378 K) within the reach of our equipment.

These results indicate that, in the case of $\mathbf{2}^{2+}$, the acetyl moiety is bulky enough to suppress the shuttling of the ring in the investigated temperature range, and that the *E*- and *Z*-isomers are transformed into one another exclusively via CN–CO bond rotation. Instead, two distinct and seemingly uncorrelated chemical processes – namely, CN–CO bond rotation and ring shuttling, are interconverting the *E* and *Z* isomeric forms of $\mathbf{1}^{2+}$. It is noteworthy that in a less polar solvent, such as $CDCl_3$, the ring shuttling motion is suppressed also in the case of $\mathbf{1}^{2+}$ (Table S4), while CN–CO rotation is slightly accelerated in line with previous observations on related amides.[52] Presumably, the less favorable solvation energy of the free triazolium stations in the less polar solvent results in a higher energetic penalty to pay for the ring to escape the station, which brings about an apparent stabilization of the reactant and product states of the shuttling process with respect to the transition state. This observation is intriguing, as it represents a remarkable example of a medium

Table 1. Rate constant and activation parameters of the isomerization processes of the investigated compounds, calculated from NMR data in DMSO-d_6

Compound	Process	k (s^{-1})[a]	$\Delta G^{\ddagger}$ (kJ mol^{-1})[b]	$\Delta H^{\ddagger}$ (kJ mol^{-1})	$\Delta S^{\ddagger}$ (J mol^{-1} K^{-1})
$\mathbf{1}^{2+}$	CN–CO rotation	4.4	73.8	30.3	–145.7
	ring shuttling	0.12	85.2	46.0	–131.3
$\mathbf{1a}^{2+}$	CN–CO rotation	1.7	79.6	54.1	–85.7
$\mathbf{1b}^{2+}$	ring shuttling	>10,000	52	24.8	–91
$\mathbf{2}^{2+}$	CN–CO rotation	29.2	72	58.3	–46
$\mathbf{2a}^{2+}$	CN–CO rotation	22.8	72	54.4	–59

[a]Determined at 338 K.
[b]Determined at 298 K

effect influencing in an opposite way two different movements within the same molecular machine. Such a "selective lubrication" arises from the specific interactions of the solvent with the different components of the MIM,[53,54] a situation that has no counterpart in macroscopic machinery.

For rotaxane $\mathbf{2}^{2+}$, a total lineshape analysis of the variable temperature (VT) NMR spectra in DMSO-d_6 and $CDCl_3$ allowed us to obtain the exchange rate constants of the CN–CO bond rotation process at different temperatures, and all the relevant kinetic activation parameters for the rotational motion of the acetyl unit were determined using an Eyring analysis (Figures S14 and S16). In the case of $\mathbf{1}^{2+}$, a more elaborate set of experiments was performed in DMSO-d_6 to deconvolute the effects of the two processes and calculate accurate kinetic parameters (Figure S10). Selective inversion recovery (SIR) experiments were performed at temperatures high enough for resonances H^c_E/H^c_Z to be in the fast exchange regime, that is, the couple of signals coalesced to a single resonance $H^c_{E/Z}$. Under these conditions, by perturbing the spin system away from equilibrium with a soft π (180°) pulse and observing the relaxation back to equilibrium of both sets of resonances $H^c_{E/Z}$ and $H^u_{E/Z}$, the rate constant of exchange between the two sites could be extracted (Table S3). Because only ring shuttling can result in intersite exchange between the $H^u_{E/Z}$ and $H^c_{E/Z}$ resonances, namely, those of the encircled and unencircled triazolium stations, the rate constant measured by SIR under these conditions reflects the exchange rate of the ring shuttling process. The exchange rate constants obtained from the SIR experiments at different temperatures were then employed as starting values for a total lineshape analysis of the VT NMR spectra of $\mathbf{1}^{2+}$ in the slow exchange regime by imposing an exchange matrix that includes two simultaneous exchange processes (CN–CO bond rotation and ring shuttling, Figure S13).[55] Indeed, as anticipated by the observation of exchanging signal pairs with a similar frequency difference but non-identical coalescence temperature, and unequivocally proved by EXSY experiments, the lineshape features in the VT spectra of $\mathbf{1}^{2+}$ could only be appropriately simulated if two simultaneous exchange processes were included. This analysis allowed to extract distinct Eyring plots and activation parameters (Table 1) for CN–CO bond rotation and ring shuttling movements. The obtained exchange rates, listed in Table 1, indicate that for $\mathbf{1}^{2+}$ about 37 rotations occur on an average between two successive shuttling events.

In order to assess the effect of the macrocycle on the rotational dynamics of the amide bond, the activation parameters for CN–CO bond rotation of rotaxanes $\mathbf{1}^{2+}$ and $\mathbf{2}^{2+}$ were compared with those of the corresponding free axles $\mathbf{1a}^{2+}$ and $\mathbf{2a}^{2+}$ (Figures 4A, 4B, S13, and S14). It is worth noting that the activation parameters for CN–CO bond rotation obtained for $\mathbf{1a}^{2+}$ and $\mathbf{2a}^{2+}$ with the same techniques

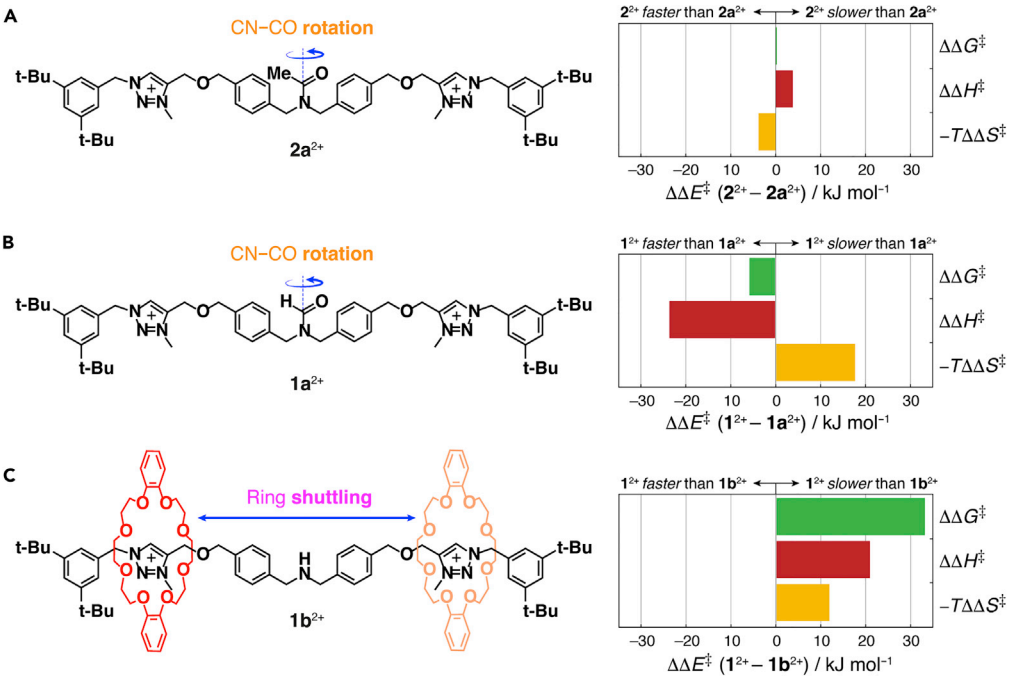

Figure 4. Activation parameters of covalent bond rotation and ring shuttling in rotaxanes and model compounds

Differences between the activation enthalpies ($\Delta\Delta H^{\ddagger}$), entropies ($-T\Delta\Delta S^{\ddagger}$), and free energies ($\Delta\Delta G^{\ddagger}$) in DMSO-$d_6$ (T = 298 K) for:

(A) CN–CO rotation in rotaxane $\mathbf{2}^{2+}$ and its free axle $\mathbf{2a}^{2+}$.

(B) CN–CO rotation in rotaxane $\mathbf{1}^{2+}$ and its free axle $\mathbf{1a}^{2+}$.

(C) Ring shuttling in rotaxane $\mathbf{1}^{2+}$ and model rotaxane $\mathbf{1b}^{2+}$.

The molecular structure of the investigated model compounds is shown in the left-hand side; the blue arrows indicate the relevant motion.

employed for the investigated rotaxanes, are in line with those reported for similar amides.[44] This proves that the other functional groups present on the axle of the investigated compounds have a negligible influence on the amide rotation (Table S4). Moreover, the enthalpies and entropies of activation determined for $\mathbf{1}^{2+}$ were compared with the activation parameters of ring shuttling measured for $\mathbf{1b}^{2+}$ (Figures 4C, S12, S15, and S17; Tables S2 and S4), a [2]rotaxane structurally identical to $\mathbf{1}^{2+}$ but devoid of the amide group, with the aim of understanding the specific effect of the formyl group on the shuttling dynamics.

The enthalpies ($\Delta H^{\ddagger}$) and entropies ($-T\Delta S^{\ddagger}$) of activation for the CN–CO bond rotation in $\mathbf{2a}^{2+}$ and $\mathbf{2}^{2+}$ are almost equal; moreover, they cancel out, leading to a negligible difference in the free energy of activation ($\Delta\Delta G^{\ddagger}$) at 298 K (Figure 4A). This observation suggests that in rotaxane $\mathbf{2}^{2+}$ the interlocked macrocycle acts essentially as a passive spectator of the CN–CO bond rotational motion, without significantly changing its conformational freedom and the magnitude of the interactions with the axle along the reaction path.

Conversely, the comparison between the activation parameters of CN–CO bond rotation in $\mathbf{1}^{2+}$ and $\mathbf{1a}^{2+}$ (Figure 4B) evidences that the presence of the ring in the rotaxane affects significantly the activation energy of the process, resulting in an overall faster rotational rate for the formyl group in $\mathbf{1}^{2+}$ than in the free axle $\mathbf{1a}^{2+}$. It is interesting to note that while the difference in activation enthalpy between $\mathbf{1}^{2+}$ and $\mathbf{1a}^{2+}$ is in favor of a faster rotation in $\mathbf{1}^{2+}$ ($\Delta\Delta H^{\ddagger}$ is negative), the activation entropy difference reveals an opposite influence ($-T\Delta\Delta S^{\ddagger}$ is positive). At room temperature, however, the enthalpic gain overcomes the entropic loss, resulting in an overall decrease in the free energy of

activation for rotaxane $\mathbf{1}^{2+}$ compared with axle $\mathbf{1a}^{2+}$. The enthalpic factor that favors a faster rotational rate in $\mathbf{1}^{2+}$ can be ascribed to a reduction of the double bond character of the amide bond in the formyl unit of the rotaxane, possibly as a consequence of CH-π interactions between the formyl hydrogen and an electron donating catechol moiety of the macrocycle.[56–59] It can be hypothesized that the large entropic penalty paid by the CN–CO bond rotation in $\mathbf{1}^{2+}$ is the result of the decreased degrees of freedom associated with the different (co-)conformations of the macrocycle—not present in the axle component $\mathbf{1a}^{2+}$—that are constrained by the torsional change of the formyl moiety along the reaction path.

The comparison between the ring shuttling activation parameters of $\mathbf{1}^{2+}$ and $\mathbf{1b}^{2+}$ (Figure 4C) evidences that the significant decrease in the rate of shuttling in the formyl-functionalized rotaxane $\mathbf{1}^{2+}$ arises from both enthalpic and entropic effects. Repulsive interactions between the carbonyl dipole and the dipoles of the crown ether oxygen atoms could destabilize[60] the transition state of shuttling in $\mathbf{1}^{2+}$ compared with $\mathbf{1b}^{2+}$; on the entropic side, a significant loss of conformational freedom can be envisaged when the macrocycle has to pass over the bulkier formyl substituent. Indeed, it has been recently reported that the possibility of undergoing threading/dethreading movements in related DB24C8-based pseudorotaxanes is determined by the ability of the macrocycle to adapt the size and shape of its cavity via room-temperature vibrations in order to accommodate a bulky molecular fragment.[61]

The dynamic behavior of rotaxane $\mathbf{1}^{2+}$ can be qualitatively summarized with the aid of a simplified three-dimensional potential energy surface (PES) diagram (Figure 5A) taking the CN–CO torsional angle of the amide group and the distance between the centroids of the ring and axle components as the reaction coordinates. The graph shows that the two experimentally observed isomerization paths in $\mathbf{1}^{2+}$ can be associated with two different reaction mechanisms that occur along orthogonal reaction coordinates, namely, CN–CO bond rotation (orange trajectories) and ring shuttling (magenta trajectories). The fact that direct automerization processes, i.e., concerted covalent bond rotation and ring shuttling, are not experimentally detected for $\mathbf{1}^{2+}$ is not surprising, because they would require a large distortion of the macrocycle cavity to enable it to pass over the formyl unit of the axle, while the CN–CO torsional angle is about 90° (gray trajectories in Figure 5A). Most likely, an activated complex of this kind, which corresponds to the red colored region in Figure 5A, constitutes a maximum in the PES of $\mathbf{1}^{2+}$.

One can imagine, however, a rotaxane related to $\mathbf{1}^{2+}$ (Figure 5B) in which, owing to specific interactions between the macrocycle and the rotor moiety, the barrier along the shuttling coordinate is decreased when the rotor is away from its minimum (I versus II). In the example illustrated in Figure 5B, the presence of the ring around the rotor also lowers the rotation barrier (I versus III). This is a particularly interesting case, as it leads to a PES topography comprising a saddle that connects four valleys, and both isomerization and automerization processes would take place by a concerted rotation-shuttling mechanism (Figure 5B, gray traces).[62] Such a scenario has significant consequences from a physico-chemical viewpoint.[63] The presence of a crossing point between the direct automerization trajectories of the *E* isomer and those of the *Z* isomer (I in Figure 5B) highlights a limitation of the Murrell-Laidler theorem,[64] which asserts that a transition state (defined as the point of maximum energy on the lowest-energy path between two stable configurations) cannot connect more than two potential energy wells. This theorem has been challenged theoretically,[65] and exceptions consisting of transformations involving small molecules with particular symmetry features have been identified.[66,67] The realization of a rotaxane like that shown in Figure 5B has yet to come, but the results described

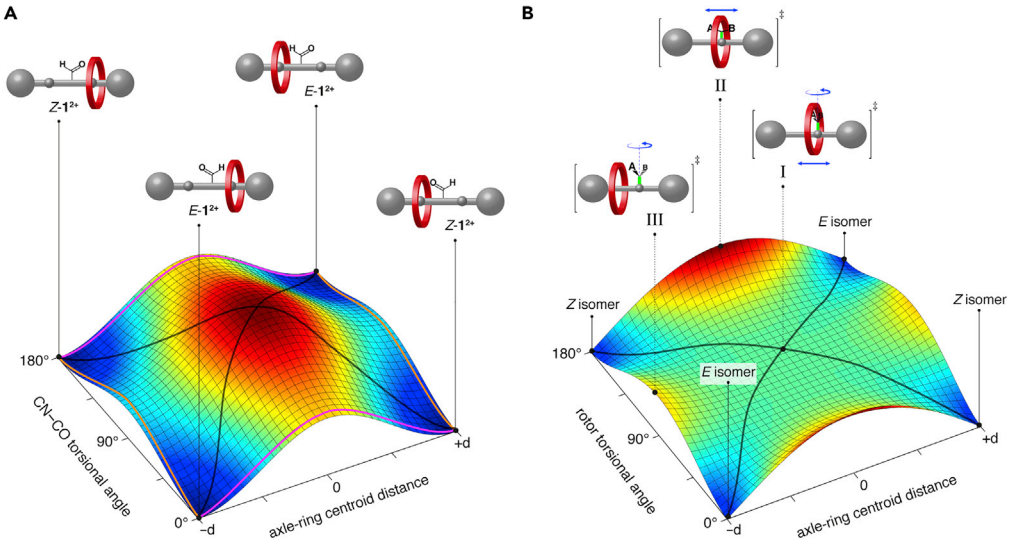

Figure 5. Representation of covalent bond rotation and ring shuttling movements with potential energy surfaces

(A) Simplified three-dimensional PES of $\mathbf{1}^{2+}$ with respect to orthogonal reaction coordinates corresponding to rotation about the CN–CO bond (orange traces) and shuttling of the ring along the axle (magenta traces). The experiments rule out the occurrence of concerted motion (gray traces), indicating that the rotation and shuttling transition states are distinct.

(B) Idealized PES and cartoon representation of a hypothetical rotaxane in which the barrier along both shuttling and rotation coordinates is lowered with respect to that for each independent motion (I versus II and III, respectively) because of specific ring-axle interactions. In such a case, the PES topography can be described as four valleys that meet at a common hilltop, which is the transition state of both *E/Z* isomerization and automerization reactions (gray trajectories). The covalent rotation and mechanical shuttling movements are simultaneous and synchronized.

here, together with the broad knowledge available on molecular recognition in MIMs, suggest that it is not an impossible task.

Another element of interest about the behavior of $\mathbf{1}^{2+}$ is related to the principle of microscopic reversibility and its corollary at equilibrium, detailed balance.[68] A popular formulation of microscopic reversibility states that the mechanism of the backward process in a reversible reaction is given by the same steps of the forward process traversed backward.[69,70] The fact that a certain rotaxane molecule can indeed be transformed from *E* to *Z*, or vice versa, by amide rotation (orange trajectories in Figure 5A) and then return to its starting isomer by shuttling (magenta trajectories), may suggest that $\mathbf{1}^{2+}$ violates the principle. This is clearly wrong because both mechanistic paths in the rotaxane have their own reverse, and on an ensemble of molecules at equilibrium the average rate for each path is equal to that of its reverse. In other words, no asymmetric flow of reagent to product is possible at equilibrium: rotation-shuttling and shuttling-rotation pathways occur with the same rate.

If, however, a non-equilibrium distribution of species is generated, then an asymmetric reactant-product flow can be achieved upon returning to equilibrium.[71] As a matter of fact, this phenomenon is observed in the EXSY experiment (Figure 3), where a non-equilibrium concentration of a species is produced via spin labeling. The evolution of the system toward the equilibrium state leads initially to a larger flow of molecules in the direction associated with the lower barrier, which is the rotation of the amide bond in the case of $\mathbf{1}^{2+}$. This is clearly reflected by the higher intensity of the off-diagonal cross-peaks related to CN–CO bond rotation compared with those of the ring shuttling movement (Figure 3B). In this context, it is also interesting to note that the ratio between the forward and backward rate constants of the shuttling and rotation processes must be the same, despite these two pathways being mechanistically different and uncorrelated.

This apparently counterintuitive constraint arises from the fact that, although two distinct and detectable reaction paths are available to the system, there is only one equilibrium condition; that is, the equilibrium constant between the *E* and *Z* stereoisomers is the same irrespective of the mechanism considered. Indeed, the peculiar isomerization of 1^{2+} constitutes a testing ground for fundamental concepts, such as microscopic reversibility, detailed balance, and their kinetic and thermodynamic consequences, and provides further demonstrations of their validity.

Conclusions

As shown recently for enatiomerism,[7,11–14,24–26] geometrical isomerism can also present novel forms of expression in MIMs as a result of their unique dynamics. We have designed, synthesized, and characterized two rotaxanes that exhibit *cis-trans* isomerism as a consequence of restricted rotation about a covalent bond on the axle component, and desymmetrization of the latter due to the presence of an interlocked macrocycle. We have identified movements involving covalent and mechanical bonds, namely, amide bond rotation and ring shuttling, as essentially independent *E/Z* isomerization mechanisms. These processes have been fully characterized in solution by applying a range of ^{1}H NMR methods and our mechanistic conclusions were supported by comparison with related model compounds. This is the first experimental demonstration of two alternative and entirely different isomerization pathways pertaining to a single stereogenic element and coexisting in an individual interlocked molecule. Such a rare phenomenon has been reported so far only for a handful of small molecules.[35–37] Interestingly, the two processes exhibit opposite rate dependence on solvent polarity; this selective lubrication effect can be exploited to tune the kinetics of the movements and thus change the relative contribution of each mechanism to the isomerization.

The concept of combining mechanostereoisomerism with conventional isomerism has a general validity as it can be applied to many thermally activated covalent movements—for example, flipping or inversion instead of rotation— and other MIMs, such as catenanes. In particular, intriguing is the possibility of using mechanical rearrangements in MIMs to affect *E/Z* isomerization reactions about double bonds which could also be photochemically activated. Indeed, the adjustment of thermal isomerization rates of molecular photoswitches by means of co-conformational movements is a new stimulating area of interest for molecular devices and machines.

Our approach not only enables access to unconventional mechanistic scenarios but is also relevant to understanding the operation of natural and artificial nanoscale machines, wherein specific reaction pathways are selected among others through the precise modulation of energy barriers.[72] Besides the fundamental interest, kinetic studies on MIMs in which different movements can take place asynchronously or synchronously are important to take synthetic molecular machines to a higher level of sophistication, where the controlled movement of a motor unit can be passed on to downstream components.[39,40,73]

EXPERIMENTAL PROCEDURES

Resource availability

Lead contact

Further information and requests for resources should be directed to and will be fulfilled by the lead contact, Alberto Credi (alberto.credi@unibo.it).

Materials availability

None of the unique compounds generated in this study are readily available.

Data and code availability

All data needed to support the conclusions of this manuscript are included in the main text or the supplemental information.

Synthesis of rotaxane 1^{2+}

Rotaxane $\mathbf{1b}H^{3+}\cdot 3PF_6^-$ (10 mg, 0.006 mmol) was dissolved in CH_2Cl_2, polymer bound 2-tertbutylimino-2-diethylamino-1,3-dimethylperhydro-1,3,2-diazaphosphorine (resin-bound BEMP) was added, and the suspension was shaken for 5 min. The resin was filtered, and the filtrate was concentrated under reduced pressure. The residue was dissolved in ethyl formate (4 mL) and refluxed for 5 days under a nitrogen atmosphere. The solution was concentrated under reduced pressure, and the residue was triturated with diethylether. The crude product was purified by size exclusion chromatography (biobeads SX-1, CH_2Cl_2) to yield $\mathbf{1}^{2+}\cdot 2PF_6^-$ as a pale-yellow solid (8 mg, 0.005 mmol, 90%). **^{1}H-NMR (500 MHz, DMSO-d$_6$, 298 K)**: δ (ppm) amide rotamer *Z*: 9.37 (s, 1H), 9.02 (s, 1H), 8.43 (s, 1H), 7.47 (s, 1H), 7.45 (s, 1H), 7.40 (s, 2H), 7.38 (d, J = 8.0 Hz, 2H), 7.36 (s, 2H), 7.23 (d, J = 7.8 Hz, 2H), 7.11–6.98 (m, 4H), 6.95–6.89 (m, 4H), 6.90–6.84 (m, 4H), 5.83 (s, 2H), 5.81 (s, 2H), 4.82 (s, 2H), 4.74 (s, 2H), 4.59 (s, 2H), 4.33–4.27 (m, 4H), 4.23 (s, 3H), 4.21 (s, 2H), 4.09 (s, 3H), 4.06–3.93 (m, 8H), 3.55 (dd, J = 11.6, 5.4 Hz, 4H), 3.51–3.42 (m, 4H), 3.27 (t, J = 4.7 Hz, 4H), 3.15 (dd, J = 10.9, 6.0 Hz, 4H), 1.28 (s, 18H), 1.22 (s, 18H). amide rotamer *E*: 9.37 (s, 1H), 9.04 (s, 1H), 8.45 (s, 1H), 7.47 (s, 1H), 7.45 (s, 1H), 7.40 (s, 2H), 7.36 (s, 2H), 7.34 (d, J = 7.8 Hz, 2H), 7.17 (d, J = 7.7 Hz, 1H), 7.11–6.98 (m, 4H), 6.95–6.89 (m, 4H), 6.90–6.84 (m, 4H), 5.84 (s, 2H), 5.81 (s, 2H), 4.83 (s, 2H), 4.70 (s, 2H), 4.61 (s, 2H), 4.33–4.27 (m, 4H), 4.24 (s, 3H), 4.19 (s, 2H), 4.08 (s, 3H), 4.06–3.93 (m, 8H), 3.55 (dd, J = 11.6, 5.4 Hz, 4H), 3.51–3.42 (m, 4H), 3.27 (t, J = 4.7 Hz, 4H), 3.15 (dd, J = 10.9, 6.0 Hz, 4H), 1.28 (s, 18H), 1.22 (s, 18H). **^{13}C-NMR (125 MHz, DMSO-d$_6$, 298 K)**: δ (ppm) mixture of *E* and *Z* rotamers: 163.2, 151.3, 147.3, 136.2, 132.0, 129.5, 128.3, 128.2, 127.8, 127.7, 127.6, 123.3, 123.0, 121.1, 120.8, 112.1, 70.4, 70.2, 69.3, 69.1, 68.7, 67.8, 56.7, 38.3, 37.4, 34.6, 34.5, 31.1, 31.0. **HRMS (ESI+)** *m/z*: $[M]^{2+}$ calcd 665.9092, found 665.9092.

Variable temperature ^{1}H NMR

^{1}H NMR spectra were recorded in DMSO-d$_6$ between 298 and 398 K, and in $CDCl_3$ between 298 and 338 K at 10 K intervals. The rates of exchange as a function of temperature were determined from visual comparisons of experimental spectra with line shapes computed using iNMR.

Selective inversion recovery ^{1}H NMR

SIR experiments were performed employing a PRESAT (Agilent) pulse sequence to selectively invert the $H^c_{E/Z}$ spin population (9.37 ppm). Calibration of the soft π (180°) pulse was achieved optimizing the pulse width. Spectra were acquired at increasing mixing times (d2) ranging from 0 to 6 s. The data of magnetization of protons $H^u_{E/Z}$ and $H^c_{E/Z}$ versus d2 were fitted using the CIFIT software to extract the chemical exchange rate constant.

SUPPLEMENTAL INFORMATION

Supplemental information can be found online at https://doi.org/10.1016/j.chempr.2021.04.010.

ACKNOWLEDGMENTS

This work was supported by the European Union's H2020 Research and Innovation Program (ERC Advanced grant n. 692981) and by the Italian Ministry of University

and Research (FARE R16S9XXKX3 and PRIN 20173L7W8K). We thank Dean Astumian, Marco Garavelli, and Giulio Ragazzon for useful discussions.

AUTHOR CONTRIBUTIONS

Conceptualization, M.B. and A.C.; investigation – synthesis, S.C. and C.d.V.; investigation – NMR, S.C. and M.B.; formal analysis, S.C. and S.S.; writing – original draft, M.B. and A.C.; writing – review and editing, S.C., M.B., and A.C.; funding acquisition, M.B., S.S., and A.C.

DECLARATION OF INTERESTS

The authors declare no competing interests.

Received: November 18, 2020
Revised: January 18, 2021
Accepted: April 19, 2021
Published: May 14, 2021

REFERENCES

1. Bruns, C.J., and Stoddart, J.F. (2016). The Nature of the Mechanical Bond: From Molecules to Machines (John Wiley & Sons).
2. Mislow, K. (1965). Introduction to Stereochemistry (Benhamin).
3. Eliel, L.E., and Wilen, H.S. (1994). Stereochemistry of Organic Compounds (Wiley).
4. Isnin, R., and Kaifer, A. (1991). E. novel class of asymmetric zwitterionic rotaxanes based on α-cyclodextrin. J. Am. Chem. Soc. *113*, 8188–8190.
5. Chiu, S.H., Elizarov, A.M., Glink, P.T., and Stoddart, J.F. (2002). Translational isomerism in a [3]catenane and a [3]rotaxane. Org. Lett. *4*, 3561–3564.
6. Fuller, A.M., Leigh, D.A., and Lusby, P.J. (2010). Sequence isomerism in [3]rotaxanes. J. Am. Chem. Soc. *132*, 4954–4959.
7. Jamieson, E.M.G., Modicom, F., and Goldup, S.M. (2018). Chirality in rotaxanes and catenanes. Chem. Soc. Rev. *47*, 5266–5311.
8. Schill, G., Rissler, K., Fritz, H., and Vetter, W. (1981). Synthesis, isolation, and identification of translationally isomeric [3]catenanes. Angew. Chem. Int. Ed. Engl. *20*, 187–189.
9. Ashton, P.R., Goodnow, T.T., Kaifer, A.E., Reddington, M.V., Slawin, A.M.Z., Spencer, N., Stoddart, J.F., Vicent, C., and Williams, D.J. (1989). A [2]Catenane made to order. Angew. Chem. Int. Ed. Engl. *28*, 1396–1399.
10. Pascu, S.I., Naumann, C., Kaiser, G., Bond, A.D., Sanders, J.K.M., and Jarrosson, T. (2007). Structures and solution dynamics of pseudorotaxanes mediated by alkali-metal cations. Dalton Trans. *35*, 3874–3884.
11. Cakmak, Y., Erbas-Cakmak, S., and Leigh, D.A. (2016). Asymmetric catalysis with a mechanically point-chiral rotaxane. J. Am. Chem. Soc. *138*, 1749–1751.
12. Dommaschk, M., Echavarren, J., Leigh, D.A., Marcos, V., and Singleton, T.A. (2019). Dynamic control of chiral space through local symmetry breaking in a rotaxane organocatalyst. Angew. Chem. Int. Ed. *58*, 14955–14958.
13. Heard, A.W., and Goldup, S.M. (2020). Synthesis of a mechanically planar chiral rotaxane ligand for enantioselective catalysis. Chem *6*, 994–1006.
14. Pairault, N., Zhu, H., Jansen, D., Huber, A., Daniliuc, C.G., Grimme, S., and Niemeyer, J. (2020). Heterobifunctional rotaxanes for asymmetric catalysis. Angew. Chem. Int. Ed. *59*, 5102–5107.
15. Li, G., Wang, L., Wu, L., Guo, Z., Zhao, J., Liu, Y., Bai, R., and Yan, X. (2020). Woven polymer networks via the topological transformation of a [2]catenane. J. Am. Chem. Soc. *142*, 14343–14349.
16. Wilson, B.H., and Loeb, S.J. (2020). Integrating the mechanical bond into metal-organic frameworks. Chem *6*, 1604–1612.
17. Takata, T. (2020). Switchable polymer materials controlled by rotaxane macromolecular switches. ACS Cent. Sci. *6*, 129–143.
18. Mena-Hernando, S., and Pérez, E.M. (2019). Mechanically interlocked materials. Rotaxanes and catenanes Beyond the small molecule. Chem. Soc. Rev. *48*, 5016–5032.
19. Balzani, V., Credi, A., and Venturi, M. (2008). Molecular Devices and Machines: Concepts and Perspectives for the Nanoworld (Wiley-VCH).
20. Qiu, Y., Song, B., Pezzato, C., Shen, D., Liu, W., Zhang, L., Feng, Y., Guo, Q.H., Cai, K., Li, W., et al. (2020). A precise polyrotaxane synthesizer. Science *368*, 1247–1253.
21. De Bo, G., Gall, M.A.Y., Kuschel, S., De Winter, J., Gerbaux, P., and Leigh, D.A. (2018). An artificial molecular machine that builds an asymmetric catalyst. Nat. Nanotechnol. *13*, 381–385.
22. Iwaso, K., Takashima, Y., and Harada, A. (2016). Fast response dry-type artificial molecular muscles with [c2]daisy chains. Nat. Chem. *8*, 625–632.
23. Wilson, M.R., Solà, J., Carlone, A., Goldup, S.M., Lebrasseur, N., and Leigh, D.A. (2016). An autonomous chemically fuelled small-molecule motor. Nature *534*, 235–240.
24. Bordoli, R.J., and Goldup, S.M. (2014). An efficient approach to mechanically planar chiral rotaxanes. J. Am. Chem. Soc. *136*, 4817–4820.
25. Corra, S., de Vet, C., Groppi, J., La Rosa, M., Silvi, S., Baroncini, M., and Credi, A. (2019). Chemical on/off switching of mechanically planar chirality and chiral anion recognition in a [2]rotaxane molecular shuttle. J. Am. Chem. Soc. *141*, 9129–9133.
26. Tian, C., Fielden, S.D.P., Pérez-Saavedra, B., Vitorica-Yrezabal, I.J., and Leigh, D.A. (2020). Single-step enantioselective synthesis of mechanically planar chiral [2]rotaxanes using a chiral leaving group strategy. J. Am. Chem. Soc. *142*, 9803–9808.
27. Neal, E.A., and Goldup, S.M. (2014). Chemical consequences of mechanical bonding in catenanes and rotaxanes: isomerism, modification, catalysis and molecular machines for synthesis. Chem. Commun. *50*, 5128–5142.
28. If the macrocycle is oriented (C_{nh}-symmetric), then mechanically planar enantiomers are also obtained; see Bordoli and Goldup.[24]
29. For the determination of *E* and *Z* configuration, the side bearing the mechanical bond has been given highest priority, according to the methodology reported for mechanical point chiral rotaxanes: Alvarez-Pérez, M., Goldup, S.M., Leigh, D.A., and Slawin, A.M.Z. (2008). A chemically-driven molecular information ratchet J. Am. Chem. Soc. *130*, 1836–1838.
30. Dünnwald, T., Parham, A.H., and Vögtle, F. (1998). Non-ionic template synthesis of amide-linked rotaxanes: axles with benzophenone and cinnamic acid units. Synthesis, 339–348.
31. Clegg, W., Gimenez-Saiz, C., Leigh, D.A., Murphy, A., Slawin, A.M.Z., and Teat, S.J.

(1999). "Smart" rotaxanes: shape memory and control in tertiary amide Peptido[2]rotaxanes. J. Am. Chem. Soc. *121*, 4124–4129.

32. Orlando, T., Salbego, P.R.S., Zimmer, G.C., Pagliari, A.B., Bender, C.R., Rodrigues, L.V., Bonacorso, H.G., Zanatta, N., Berná, J., and Martins, M.A.P. (2018). Conformer distribution in rotaxanes containing nonsymmetric threads: a systematic approach. Eur. J. Org. Chem. 4978–4990.

33. Kihara, N., Koike, Y., and Takata, T. (2007). Effect of steric barrier on the shuttling of rotaxane having crown ether wheel. Chem. Lett. *36*, 208–209.

34. Salem, L. (1971). Narcissistic reactions. Synchronism vs. nonsynchronism in automerizations and enantiomerizations. Acc. Chem. Res. *4*, 322–328.

35. Gillick-Healy, M.W., Jennings, E.V., Müller-Bunz, H., Ortin, Y., Nikitin, K., and Gilheany, D.G. (2017). Two independent orthogonal stereomutations at a single asymmetric center: a narcissistic couple. Chem. Eur. J. *23*, 2332–2339.

36. Strawczynski, A., Ros, R., and Roulet, R. (1988). Intramolecular dynamics of tetranuclear iridium carbonyl cluster compounds. Part 1. Bromotri-M-carbonyloctacarbonyltetrairidate(1-). Helv. Chim. Acta *71*, 867–871.

37. Gromova, M., Jarjayes, O., Hamman, S., Nardin, R., Béguin, C., and Willem, R. (2000). Quantitative 2D EXSY and dynamic ^{19}F-NMR studies of the dynamic behaviour of the bidentate chelate complex $Ga(fox)_3$ (fox = 5-fluoro-8-hydroxyquinoline). Ber. Dtsch. Chem. Ges. 545–550.

38. Iwamura, H., and Mislow, K. (1988). Stereochemical consequences of dynamic gearing. Acc. Chem. Res. *21*, 175–182.

39. Štacko, P., Kistemaker, J.C.M., van Leeuwen, T., Chang, M.C., Otten, E., and Feringa, B.L. (2017). Locked synchronous rotor motion in a molecular motor. Science *356*, 964–968.

40. Baroncini, M., and Credi, A. (2017). Gearing up molecular rotary motors. Science *356*, 906–907.

41. Carreras, A., Fuligni, L., Alemany, P., Llunell, M., Bofill, J.M., and Quapp, W. (2019). Conformational analysis of enantiomerization coupled to internal rotation in Triptycyl-N-Helicenes. Phys. Chem. Chem. Phys. *21*, 11395–11404.Uhl, E., Thumser, S., Mayer, P., and Dube, H. (2018). Transmission of unidirectional molecular motor rotation to a remote biaryl axis. Angew. Chem. Int. Ed. *57*, 11064–11068.

42. Erbland, G., Abid, S., Gisbert, Y., Saffon-Merceron, N., Hashimoto, Y., Andreoni, L., Guérin, T., Kammerer, C., and Rapenne, G. (2019). Star-shaped ruthenium complexes as prototypes of molecular gears. Chem. Eur. J. *25*, 16328–16339.

43. Coutrot, F. (2015). A focus on triazolium as a multipurpose molecular station for pH-sensitive interlocked crown-ether-based molecular machines. ChemistryOpen *4*, 556–576.

44. Stewart, W.E., and Siddall, T.H. (1970). Nuclear magnetic resonance studies of amides. Chem. Rev. *70*, 517–551.

45. Liebman, J.F., and Greenberg, A. (1974). The origin of rotational barriers in amides and esters. Biophys. Chem. *1*, 222–226.

46. Drakenberg, T., and Forsén, S. (1970). Barrier to internal rotation of amides. I. Formamide. J. Phys. Chem. *74*, 1–7.

47. Chao, S., Romuald, C., Fournel-Marotte, K., Clavel, C., and Coutrot, F. (2014). A strategy utilizing a recyclable macrocycle transporter for the efficient synthesis of a triazolium-based [2] rotaxane. Angew. Chem. Int. Ed. *53*, 6914–6919.

48. Young, P.G., Hirose, K., and Tobe, Y. (2014). Axle length does not affect switching dynamics in degenerate molecular shuttles with rigid spacers. J. Am. Chem. Soc. *136*, 7899–7906.

49. Bragg, R.A., Clayden, J., Morris, G.A., and Pink, J.H. (2002). Stereodynamics of bond rotation in tertiary aromatic amides. Chem. Eur. J. *8*, 1279–1289.

50. McGlinchey, M. (2014). Symmetry breaking in NMR spectroscopy: the elucidation of hidden molecular rearrangement processes. Symmetry *6*, 622–654.

51. Nikitin, K., and O'Gara, R. (2019). Mechanisms and beyond: elucidation of fluxional dynamics by exchange NMR spectroscopy. Chem. Eur. J. *25*, 4551–4589.

52. Wiberg, K.B., Rablen, P.R., Rush, D.J., and Keith, T.A. (1995). Amides. 3. Experimental and theoretical studies of the effect of the medium on the rotational barriers for N,N-dimethylformamide and n,n-dimethylacetamide. J. Am. Chem. Soc. *117*, 4261–4270.

53. Panman, M.R., Bakker, B.H., den Uyl, D., Kay, E.R., Leigh, D.A., Buma, W.J., Brouwer, A.M., Geenevasen, J.A., and Woutersen, S. (2013). Water lubricates hydrogen-bonded molecular machines. Nat. Chem. *5*, 929–934.

54. Fu, H., Shao, X., Chipot, C., and Cai, W. (2017). The lubricating role of water in the shuttling of rotaxanes. Chem. Sci. *8*, 5087–5094.

55. Morris, K.F., and Erickson, L.E. (1996). NMR determination of internal rotation rates and rotational energy barriers: a physical chemistry lab project. J. Chem. Educ. *73*, 471–473.

56. Pluth, M.D., Bergman, R.G., and Raymond, K.N. (2008). Acceleration of amide bond rotation by encapsulation in the hydrophobic interior of a water-soluble supramolecular assembly. J. Org. Chem. *73*, 7132–7136.

57. Umemoto, K., and Ouchi, K. (1985). Hindered internal rotation and intermolecular interactions. Proc. Indian Acad. Sci. (Chem. Sci.) *94*, 1–119.

58. Hirota, M., Sakaibara, K., Suezawa, H., Yuzuri, T., Ankai, E., and Nishio, M. (2000). Intramolecular CH-π interaction. Substituent effect as a probe for hydrogen bond-like character. J. Phys. Org. Chem. *13*, 620–623.

59. In principle, such an interaction could lead to a stabilization of the *E* isomer with respect to the other one; in practice, the effect on the *E-Z* equilibrium is likely too small to cause a measurable difference in the concentration of the two isomers.

60. Li, H., Zhu, Z., Fahrenbach, A.C., Savoie, B.M., Ke, C., Barnes, J.C., Lei, J., Zhao, Y.L., Lilley, L.M., Marks, T.J., et al. (2013). Mechanical bond-induced radical stabilization. J. Am. Chem. Soc. *135*, 456–467.

61. Groppi, J., Casimiro, L., Canton, M., Corra, S., Jafari-Nasab, M., Tabacchi, G., Cavallo, L., Baroncini, M., Silvi, S., Fois, E., and Credi, A. (2020). Precision molecular threading/dethreading. Angew. Chem. Int. Ed. *59*, 14825–14834.

62. Collins, P., Ezra, G.S., and Wiggins, S. (2011). Index k saddles and dividing surfaces in phase space with applications to isomerization dynamics. J. Chem. Phys. *134*, 244105.

63. Pradhan, R., and Lourderaj, U. (2019). Can reactions follow non-traditional second-order saddle pathways avoiding transition states? Phys. Chem. Chem. Phys. *21*, 12837–12842.

64. Murrell, J.N., and Laidler, K.J. (1968). Symmetries of activated complexes. Trans. Faraday Soc. *64*, 371–377.

65. Wales, D.J., and Berry, R.S. (1992). Limitations of the Murrell-Laidler theorem. J. Chem. Soc. Faraday Trans. *88*, 543–544.

66. Mauksch, M., and Schleyer, P.R. (2001). Effective monkey saddle points and berry and lever mechanisms in the topomerization of SF_4 and related tetracoordinated AX_4 species. Inorg. Chem. *40*, 1756–1769.

67. Martin Birney, D.M. (2010). Theory, experiment and unusual features of potential energy surfaces of pericyclic and pseudopericyclic reactions with sequential transition structures. Curr. Org. Chem. *14*, 1658–1668.

68. Tolman, R.C. (1925). The principle of microscopic reversibility. Proc. Natl. Acad. Sci. USA *11*, 436–439.

69. Moore, J.W., and Pearson, R.G. (1981). The Principle of Microscopic Reversibility - Free Energy Profiles. In Kinetics and Mechanism, Third Edition (Wiley), pp. 372–373.

70. Gold, V., Loening, K.L., McNaught, A.D., and Shemi, P. (1997). IUPAC Compendium of Chemical Terminology, Second Edition (Blackwell Science).

71. Wolfe, S., Schlegel, H.B., Csizmadia, I.G., and Bernardi, F. (1975). Chemical dynamics of symmetric and asymmetric reaction coordinates. J. Am. Chem. Soc. *97*, 2020–2024.

72. Astumian, R.D. (2018). Trajectory and cycle-based thermodynamics and kinetics of molecular machines: the importance of microscopic reversibility. Acc. Chem. Res. *51*, 2653–2661.

73. Wilson, B.H., Vojvodin, C.S., Gholami, G., Abdulla, L.M., O'Keefe, C.A., Schurko, R.W., and Loeb, S.J. (2021). Precise spatial arrangement and interaction between two different mobile components in a metal-organic framework. Chem *7*, 202–211.